



## Open Archive Toulouse Archive Ouverte (OATAO)

OATAO is an open access repository that collects the work of some Toulouse researchers and makes it freely available over the web where possible.

This is an author's version published in: <http://oatao.univ-toulouse.fr/20236>

**Official URL:** <https://onlinelibrary.wiley.com/doi/abs/10.1002/chem.201403819>

### To cite this version:

Zhang, Xuewei and Cardozo Perez, Andrés Fernando and Chen, Si and Zhang, Wenjing and Julcour-Lebigue, Carine and Lansalot, Muriel and Blanco, Jean-François and Gayet, Florence and Delmas, Henri and Charleux, Bernadette and Manoury, Eric and D'Agosto, Franck and Poli, Rinaldo Core-shell nanoreactors for efficient aqueous biphasic catalysis. (2014) *Chemistry A European Journal*, 20. 15505-15517. ISSN 1521-3765

Any correspondence concerning this service should be sent to the repository administrator:

[tech-oatao@listes-diff.inp-toulouse.fr](mailto:tech-oatao@listes-diff.inp-toulouse.fr)

# Core–Shell Nanoreactors for Efficient Aqueous Biphasic Catalysis

Xuwei Zhang,<sup>[b]</sup> Andrés F. Cardozo,<sup>[c, d]</sup> Si Chen,<sup>[a, d]</sup> Wenjing Zhang,<sup>[b]</sup> Carine Julcour,<sup>[c, d]</sup> Muriel Lansalot,<sup>[b]</sup> Jean-François Blanco,<sup>[c, d]</sup> Florence Gayet,<sup>[a, d]</sup> Henri Delmas,<sup>[c, d]</sup> Bernadette Charleux,<sup>[b, e]</sup> Eric Manoury,<sup>\*[a, d]</sup> Franck D'Agosto,<sup>\*[b]</sup> and Rinaldo Poli <sup>\*[a, d, e]</sup>

**Abstract:** Water-borne phosphine-functionalized core-cross-linked micelles (**CCM**) consisting of a hydrophobic core and a hydrophilic shell were obtained as stable latexes by reversible addition–fragmentation chain transfer (RAFT) in water in a one-pot, three-step process. Initial homogeneous aqueous-phase copolymerization of methacrylic acid (MAA) and poly(ethylene oxide) methyl ether methacrylate (PEOMA) is followed by copolymerization of styrene (S) and 4-diphenylphosphinostyrene (DPPS), yielding P(MAA-co-PEOMA)-*b*-P(S-co-DPPS) amphiphilic block copolymer micelles (**M**) by polymerization-induced self-assembly (PISA), and final micellar cross-linking with a mixture of S and diethylene glycol dimethacrylate. The **CCM** were characterized by dynamic light scattering and NMR spectroscopy to evaluate size, dispersity, stability, and the swelling ability of various organic sub-

strates. Coordination of [Rh(acac)(CO)<sub>2</sub>] (acac = acetylacetonate) to the core-confined phosphine groups was rapid and quantitative. The **CCM** and **M** latexes were then used, in combination with [Rh(acac)(CO)<sub>2</sub>], to catalyze the aqueous biphasic hydroformylation of 1-octene, in which they showed high activity, recyclability, protection of the activated Rh center by the polymer scaffold, and low Rh leaching. The **CCM** latex gave slightly lower catalytic activity but significantly less Rh leaching than the **M** latex. A control experiment conducted in the presence of the sulfoxantphos ligand pointed to the action of the **CCM** as catalytic nanoreactors with substrate and product transport into and out of the polymer core, rather than as a surfactant in interfacial catalysis.

## Introduction

Despite the several advantages offered by heterogeneous catalysis in industrial catalyzed processes, homogeneous catalysis remains attractive in terms of activity and selectivity. One of the outstanding challenges in this area is to develop efficient protocols for continuous-flow production with total catalyst recovery and recycling.<sup>[1]</sup> Different strategies for catalyst recovery include distillation, precipitation, extraction, and ultrafiltration through permselective membranes. Without doubt, the least costly and most easily implemented process is decantation, provided that the catalyst and the reaction product are in two different liquid phases at the end of the transformation and decantation is rapid. It is even better if an extraction solvent can be avoided by developing biphasic catalytic protocols in which one liquid phase contains the substrate/product and the catalyst is confined in a different liquid phase, but in this case mass transport becomes a major issue. Although the use of fluorinated organic solvents<sup>[2]</sup> and ionic liquids<sup>[3]</sup> for catalyst confinement has attracted a great deal of attention, water remains the most interesting choice in view of its lower cost and hazards.<sup>[4]</sup>

There are essentially three different approaches to homogeneous biphasic catalysis. The first scenario involves reaction in the bulk of the catalyst phase. The substrate must be sufficiently soluble in the catalyst phase, which severely limits this approach, especially for aqueous biphasic systems. The most


[a] S. Chen, Dr. F. Gayet, Dr. E. Manoury, Prof. R. Poli  
CNRS, LCC (Laboratoire de Chimie de Coordination)  
205 route de Narbonne, BP 44099  
31077, Toulouse CEDEX 4 (France)  
E-mail: eric.manoury@lcc-toulouse.fr  
rinaldo.poli@lcc-toulouse.fr

[b] Dr. X. Zhang, Dr. W. Zhang, Dr. M. Lansalot, Prof. B. Charleux,  
Dr. F. D'Agosto  
Université de Lyon, Univ. Lyon 1, CPE Lyon  
CNRS, UMR 5265, C2P2 (Chemistry, Catalysis, Polymers &  
Processes), Team LCPP  
Bat 308F, 43 Bd du 11 Novembre 1918  
69616 Villeurbanne (France)  
E-mail: franck.dagosto@univ-lyon1.fr

[c] Dr. A. F. Cardozo, Dr. C. Julcour, Dr. J.-F. Blanco, Prof. H. Delmas  
CNRS, LGC (Laboratoire de Génie Chimique)  
4 Allée Emile Monso, BP 84234  
31030 Toulouse Cedex 4 (France)

[d] Dr. A. F. Cardozo, S. Chen, Dr. C. Julcour, Dr. J.-F. Blanco, Dr. F. Gayet,  
Prof. H. Delmas, Dr. E. Manoury, Prof. R. Poli  
Université de Toulouse, UPS, INPT  
31077, Toulouse Cedex 4 (France)

[e] Prof. B. Charleux, Prof. R. Poli  
Institut Universitaire de France  
103 bd Saint-Michel, 75005, Paris (France)

 Supporting information for this article is available on the WWW under  
<http://dx.doi.org/10.1002/chem.201403819>.

relevant example is Rh-catalyzed hydroformylation with water-soluble phosphines as supporting ligands,<sup>[5]</sup> which is operated on a large industrial scale ( $>8 \times 10^5 \text{ t a}^{-1}$ ). However, this process is limited to propene and butene, because higher  $\alpha$ -olefins are insufficiently water soluble and give low, mass-transport-limited conversion rates. Additives such as cosolvents (e.g., alcohols)<sup>[6]</sup> and cyclodextrins<sup>[7]</sup> have been used to improve the solubility of the substrate in the aqueous phase.

A second approach consists of transferring the catalyst reversibly to the substrate/product phase, but in this case the key problem is how to avoid significant catalyst losses at the separation stage. An interesting approach is that of anchoring the homogeneous catalyst to thermomorphic polymers that are completely water soluble at room temperature but become more lipophilic and migrate toward the organic phase at the higher temperatures used for the catalytic reaction.<sup>[8]</sup> Then, when the solution is cooled back to room temperature at the end of the reaction, the catalyst migrates more or less completely back to the aqueous phase.

The third approach is micellar catalysis.<sup>[9]</sup> In the most intensively investigated aqueous biphasic protocol, the catalyst is anchored to the hydrophobic part of surfactants that self-organize as micellar nanoreactors when their concentration is greater than the critical micelle concentration (CMC). In this approach, the reaction occurs in the hydrophobic core of the micelles, which are themselves confined in water. Mass transport is not rate-limiting and a variety of easily synthesized surfactants is available for this elegant approach. In particular, use of amphiphilic block copolymers that self-assemble into micelles in water yields objects that are not only kinetically more stable than surfactant-based micelles, but also provide a wider choice of micellar supports for the catalyst in terms of chemical nature of the hydrophobic and hydrophilic environment and size tunability.<sup>[10]</sup> However, two major limitations are the formation of stable emulsions by excessive swelling of the micellar core and catalyst loss, even for surfactants that have a very low CMC.

It is conceptually possible to remove both limitations by turning the self-organized micellar architecture into a unimolecular core-shell nano-object by cross-linking all surfactant molecules, so that swelling of the particles is limited. Recent developments in reversible-deactivation radical polymerization (RDRP) now allow the formation of polymer particles with elaborate and precise architectures, including unimolecular core-shell polymers with narrow size dispersity.<sup>[11]</sup> A few of these have already been used as nanoreactors for catalytic applications.<sup>[10]</sup> O'Reilly et al. have developed nanoreactors containing a hydrophilic poly(acrylic acid) (PAA) shell and a hydrophobic polystyrene (PS) core in which catalytic  $\text{Cu}^I$  centers are coordinated to terpyridine ligands. After micellization of the preformed PAA-*b*-PS amphiphilic block copolymers and shell cross-linking by reaction with a diamine, these objects were applied to the Cu-catalyzed Huisgen alkyne-azide cycloaddition under homogeneous conditions (DMF/ $\text{H}_2\text{O}$  mixed solvent).<sup>[12]</sup> Weck et al. have developed amphiphilic A-B-C tri-block polyoxazolines with a hydrophilic A block, a photo-cross-linkable B block, and a C block functionalized with an enantio-

merically pure salen ligand. After photo-cross-linking of the B shell and metalation of the C core with  $\text{Co}^{III}$ , they were applied as catalytic nanoreactors in the hydrolytic kinetic resolution of epoxides and successfully recycled by ultrafiltration.<sup>[13]</sup> These objects showed slightly lower catalytic activity than analogous non-cross-linked objects due to a less permeable shell in the cross-linked particles. In principle, mass transport should be less affected, or not at all, by cross-linking at the hydrophobic end of the surfactant or amphiphilic polymer (Figure 1). To the best of our knowledge, this polymeric architecture has not yet been elaborated for application as catalytic nanoreactor, with the catalyst located on flexible linear arms in a unimolecular core-shell nano-object.

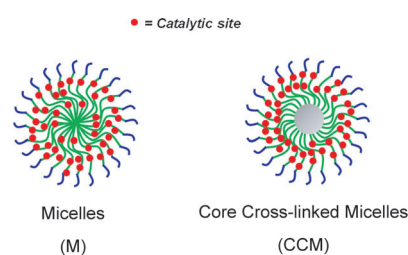


**Figure 1.** Transposition of the micellar catalysis concept to a unimolecular core-shell nano-object.

The closest related example is a phosphine-functionalized core-shell polymer prepared by Sawamoto et al. by  $[\text{RuCl}_2(\text{PPh}_3)_3]$ -catalyzed atom-transfer radical polymerization (ATRP). A convergent synthetic strategy was applied, starting with hydrophilic and thermoresponsive chains made from poly(ethylene oxide) methyl ether methacrylate (PEOMA) monomer, which were subsequently extended with the ligand monomer 4-diphenylphosphinostyrene (DPPS) and simultaneously cross-linked with ethylene glycol dimethacrylate (EGDMA).<sup>[14]</sup> Because of the synthetic methodology, the ATRP catalyst remained entrapped in the nanoreactor core, coordinated to the phosphine groups, although it was possible to subsequently demetalate the polymer.<sup>[15]</sup> These objects were applied to Ru-catalyzed transfer hydrogenation in a thermomorphic approach.<sup>[16]</sup> Hence, in these nano-objects the anchoring sites for the catalyst are located inside a cross-linked network rather than on flexible arms. Our target nanoreactors differ from the polymers described by Sawamoto et al. in two additional ways: 1) the hydrophilic shell is designed to limit or completely avoid transfer of the nano-objects to the organic phase at the operational temperature of the catalytic application and 2) since we wished to develop nanoreactors for potential general use with any catalytic metal, we selected a methodology giving direct access to a metal-free polymer.

To synthesize the target nanoreactors we considered RDRP in dispersed media. Recent progress has shown that this methodology allows the formation of polymer particles exclusively composed of well-defined amphiphilic block copolymers.<sup>[17]</sup> In the particular field of emulsion polymerization, the strategy relies on the use of hydrophilic macromolecular chains carrying a reactivable extremity that enables their further extension by

the polymerization in water of a hydrophobic monomer. The formation of this insoluble segment leads to the self-assembly of the block copolymers with formation of micellar nanoparticles self-stabilized by their hydrophilic block. This polymerization-induced self-assembly (PISA) approach in emulsion polymerization is currently at the heart of many studies using mainly reversible addition-fragmentation chain transfer (RAFT).<sup>[17a,18]</sup> A wide range of morphologies (spheres, nanofibers, vesicles) can be obtained in higher yield (> 30% solids content)<sup>[18b,c,e,f,h]</sup> compared to the conventional self-assembly of preformed amphiphilic block copolymers.<sup>[19]</sup>

The use of a controlled radical polymerization technique to grow each block successively is a perfect tool to accurately control the chaining of the monomer units. Thus, combining the best attributes of RDRP in water and the use of polymerization in dispersed media allows full control of the structure of the final nano-object from the extremity of the stabilizing layer to the very heart of the particle. We thus anticipated that the design of spherical nanoparticles as alternatives to the nano-reactors used in micellar catalysis of hydroformylation could be possible. To this end, we performed the RAFT copolymerization of methacrylic acid (MAA) with PEOMA to generate a P(MAA-co-PEOMA) macromolecular RAFT agent (macroRAFT) in water on the basis of our expertise in the field.<sup>[18c,f,h]</sup> In a second step and in the same reactor, styrene (S) and DPPS were added to generate P(MAA-co-PEOMA)-*b*-P(S-co-DPPS) amphiphilic block copolymers that self-assembled into nanometric micellar particles. Finally, subsequent addition of a cross-linker, namely, diethylene glycol dimethacrylate (DEGDMA) allowed the generation of stable and core-cross-linked particles that incorporate the triphenylphosphine ligand. These particles were evaluated in terms of mass transport of organic molecules across the hydrophilic barrier, coordination chemistry with a typical hydroformylation precatalyst, namely, [Rh(acac)(CO)<sub>2</sub>] (acac = acetylacetonate), and efficiency as catalytic nano-reactors. For this purpose we selected the aqueous biphasic hydroformylation of 1-octene as a proof-of-principle application, although we believe that this novel approach offers wider perspectives in aqueous biphasic catalysis.

## Results and Discussion

### Synthesis of core-shell nano-reactors

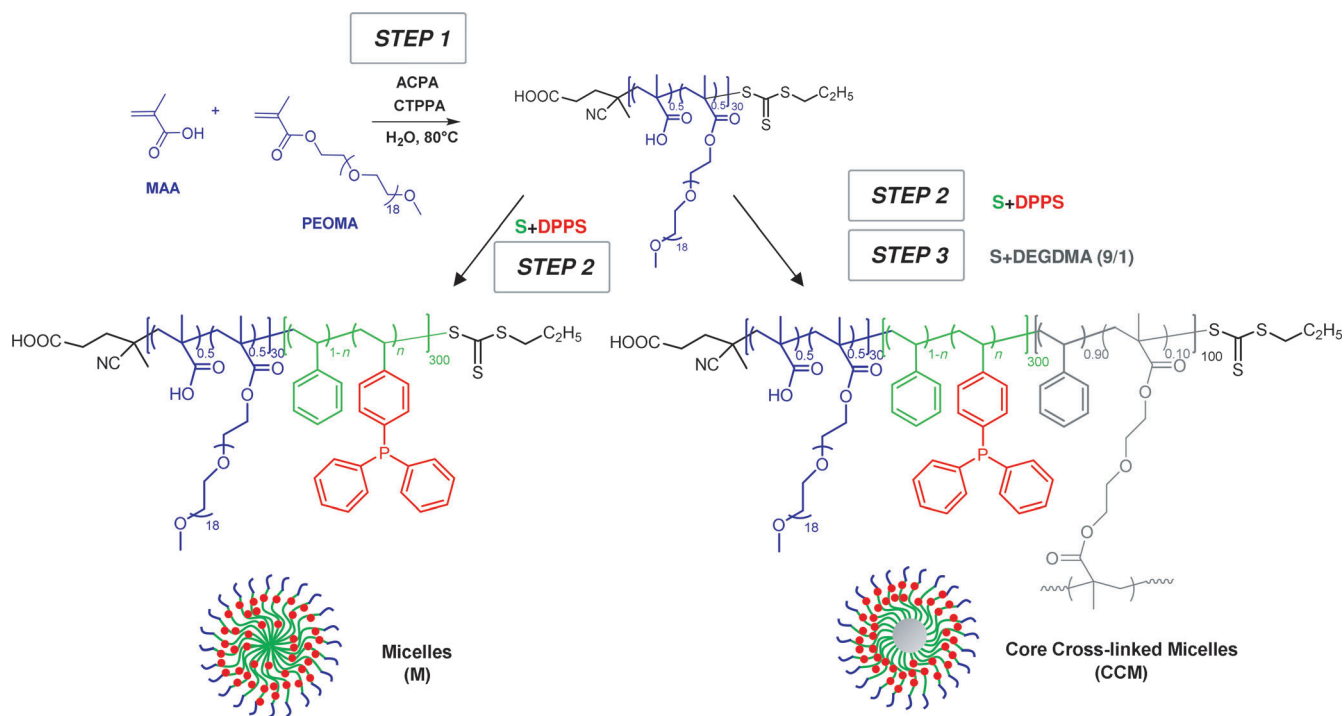
In our recent investigations, poly(methacrylic acid-co-poly(ethylene oxide) methyl ether methacrylate) hydrophilic statistical copolymers carrying a trithiocarbonate (TTC) end group (P(MAA-co-PEOMA)-TTC) were synthesized in water by RAFT. They were then employed as macroRAFT agents in the RAFT emulsion polymerization of hydrophobic monomers to obtain stable latex particles exclusively composed of well-defined amphiphilic block copolymers.<sup>[18a-c,f,h]</sup>

Some controlled radical cross-linking copolymerizations have been depicted as being PISA processes in which a cross-linker is used alone or during the polymerization of a monomer in the presence of a soluble macroRAFT agent.<sup>[11b,20]</sup> Depending on the amount of employed cross-linker, nanogels or core-cross-linked micelles were obtained.<sup>[21]</sup> However, if the addition of the cross-linker is delayed relative to the addition of a hydrophobic monomer, an original morphology should also be obtained in which a non-cross-linked hydrophobic layer can be formed first and can surround a hydrophobic cross-linked core. We thus took advantage of this strategy in water to target two types of nanoparticles carrying a P(MAA-co-PEOMA) (MAA/PEOMA = 1/1,  $M_n = 16\,200\text{ g mol}^{-1}$ , dispersity  $\mathcal{D} = 1.1$ ) shell and cores incorporating S and DPPS ([S]/[DPPS] = 90/10, number-average degree of polymerization ( $DP_n$ ) = 400), non-cross-linked or cross-linked with DEGDMA (Table 1 and Scheme 1). The first type of nanoparticles obtained without DEGDMA are simple micelles (**M**) resulting from the self-assembly of P(MAA-co-PEOMA)-*b*-P(S-co-DPPS) during polymerization. The second type are core-cross-linked micelles (**CCM**) obtained by the polymerization of a first batch of S and DPPS ([S]/[DPPS] = 90/10,  $DP_n = 300$ ), directly followed by the polymerization of DEGDMA and S ([S]/[DEGDMA] = 90/10,  $DP_n = 100$ ). The detailed experimental conditions and the characteristics of the final products are listed in Table 1. In all the experiments, the pH was not adjusted (pH 3.5). Conversions were almost quantitative for each step of the process. For comparison purposes, a phosphine-free **CCM** latex was also synthesized under the same experimental conditions (DPPS replaced by the equivalent amount of S in the synthetic procedure; see Supporting Information, Table S1 for details).

**Table 1.** Results of the one-pot RAFT emulsion polymerizations of styrene and DPPS in the presence of P(MAA-co-PEOMA)-TTC macroRAFT agent in water at 80 °C and pH 3.5.

Run	Step 1		Step 2				Step 3								
	$M_{n,SEC}^{[a]}$ [g mol <sup>-1</sup> ]	$\mathcal{D}^{[a]}$	$DP_n$	[S] <sub>0</sub> /[DPPS] <sub>0</sub>	Conv. [%] <sup>[b]</sup>	$M_{n,theo}^{[c]}$ [g mol <sup>-1</sup> ]	$M_{n,SEC}^{[a]}$ [g mol <sup>-1</sup> ]	$\mathcal{D}^{[a]}$	$D_z$ [nm] /PD <sup>[d]</sup>	$DP_n$	[S] <sub>0</sub> / [DEGDMA] <sub>0</sub>	Conv. [%] <sup>[b]</sup>	$D_z$ [nm]/PD <sup>[d]</sup> H <sub>2</sub> O	THF	
1: <b>M</b>		1.11	300	90/10	100	100	53 200	44 600	1.48	83/0.11	100	100/0	97	72/0.21	–
2: <b>CCM</b>	16 200	1.11	300	90/10	97	100	52 100	52 300	1.51	76/0.11	100	90/10	100	79/0.18	175/0.28

[a] Measured by SEC in DMF with polystyrene standards for step 2. [b] The conversion of styrene was determined by gravimetric analysis and that of DPPS was measured by <sup>31</sup>P NMR spectroscopy in [D<sub>2</sub>O]THF. [c] The theoretical molar mass of copolymers was calculated by using the following equation:  $M_{n,theo} = ([M]_0/[macroRAFT]_0) \times \text{molar mass of monomer} \times \text{conversion} / 100 + M_{n,macroRAFT}$ . [d] For the determination of  $D_z$  in THF, the latex was concentrated before dilution in THF. Solids content: 26.5 and 27.3 wt% for **M** and **CCM**, respectively.



**Scheme 1.** General strategy of RAFT-mediated emulsion polymerization for the synthesis of various types of core-shell nano-reactors.

### Characterization of the core-shell nano-objects

The molar masses of the copolymers were measured by size-exclusion chromatography (SEC) in DMF prior to cross-linking. The complete shift of the SEC peak compared with that of the macroRAFT while maintaining a narrow molar mass distribution indicated total consumption of the macroRAFT and formation of the targeted block copolymers. The particle size of the final dispersions, both before and after cross-linking, was measured by dynamic light scattering (DLS) in water, as well as in THF for the cross-linked particles. The z-average particle sizes  $D_z$  are in the range 70–80 nm in water (Table 1) for both **M** and **CCM**. The **CCM** swell by a factor of about 2 in diameter (8 in volume) in THF. The spherical morphology was in all cases confirmed by TEM observations (Figure 2).

The incorporation of DPPS was confirmed by  $^1\text{H}$  and  $^{31}\text{P}\{^1\text{H}\}$  NMR spectroscopic analysis of the final dispersions in  $[\text{D}_8]\text{THF}$ , which is a good solvent for all of the polymer constituents. The  $^1\text{H}$  NMR spectrum of **CCM** is shown in Figure 3a (see Figure S1 in the Supporting Information for further data). These

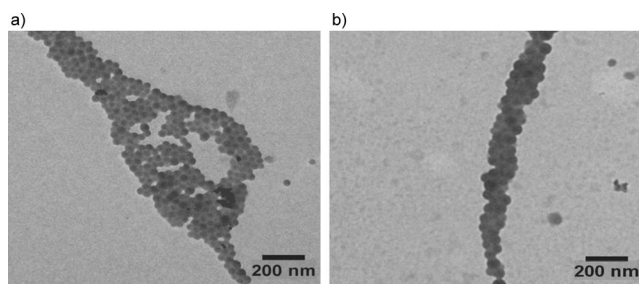


**Figure 2.** TEM images of a) **M** and b) **CCM**.

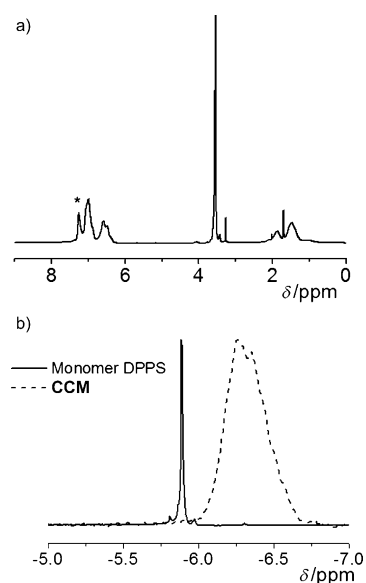


**Figure 3.** a)  $^1\text{H}$  NMR spectra of **CCM** in  $[\text{D}_8]\text{THF}$ . The star indicates the resonance of the aromatic protons of the DPPS units. b)  $^{31}\text{P}\{^1\text{H}\}$  NMR spectra of DPPS monomer and **CCM** in  $[\text{D}_8]\text{THF}$ .

studies were made possible by the cross-linked core structure, which allowed their manipulation in organic solvent while keeping their integrity. The incorporation of the DPPS units is shown by the presence of the resonance of the aromatic protons of the triphenylphosphine moiety at  $\delta = 7.2$  ppm (indicated by a star in Figure 3a). On calibrating the intensity of the resonance at  $\delta = 3.7$  ppm corresponding to the methylene protons of the PEO side chains to unity ( $I_{\text{PEO}} = 1$ ), the integrated area of the aromatic protons in the region  $\delta = 7.5$ – $6.2$  ppm

( $I_{\text{arom}} = 1.06$ ) was found to be substantially lower than the theoretical value of 1.74, which can be calculated from the molar ratio of the monomers used in the polymer synthesis, namely, PEOMA on the one hand and a combination of S and DPPS on the other. The discrepancy may be partially due to the loss of response for the aromatic protons related to the longer longitudinal relaxation time  $T_1$ , but the major reason is confinement of part of the styrene units in the cross-linked core during step 3 of the synthesis. This view is fully supported by the analogous measurement of the relative intensity of the same signals in the **M** sample, in which all components are mobile. For this sample the measured integral ratio (1.72, both with a standard 1 s relaxation delay and with a 30 s delay) is closer to the theoretical ratio of 2.00. The smaller and sharp resonance at  $\delta = 3.3$  ppm corresponds to the OMe group at the end of the PEO chains, and its integrated intensity relative to  $I_{\text{PEO}}$  matches with the known molar mass of PEO in the PEOMA monomer. Further analyses were performed by  $^{31}\text{P}\{^1\text{H}\}$  NMR spectroscopy (Figure 3b). The phosphorus resonance ( $\delta = -5.9$  ppm) is narrow for DPPS monomer and broadened and shifted in the polymer structure ( $\delta = -6.2$  ppm). The displacement of the  $^{31}\text{P}$  NMR resonance on incorporation of the DPPS monomer in the polymer is a convenient probe for monitoring DPPS consumption during polymerization.

One important question is whether the cross-linking reaction is complete. Since any non-cross-linked arms would certainly remain trapped in the nano-objects, neither the microscopic characterization nor the standard NMR spectra provide any information on this issue. We therefore resorted to DOSY NMR spectroscopy, which allows the determination of diffusion coefficients through investigation of translation by Brownian motion.<sup>[22]</sup> For the pristine latex in water, only the methylene and terminal OMe signals of PEO are observable (see also further discussion below) and lead to DOSY NMR responses, which allowed evaluation of the diffusion coefficient of the nano-objects in the range  $(6.1\text{--}6.8)\times 10^{-11} \text{ m}^2 \text{ s}^{-1}$ . The self-diffusion coefficient of water of  $(1.6 \pm 0.2)\times 10^{-9} \text{ m}^2 \text{ s}^{-1}$  was used in each experiment for internal calibration. No other responses were observed within the sensitivity of the experiment, that is, no residual monomer or non-cross-linked free arms were present in the aqueous phase, as expected. In  $[\text{D}_8]\text{THF}$  solution, however, any residual monomer and non-cross-linked arm would be fully solvated, become independent of the larger nano-objects, and yield separate DOSY NMR responses. The DOSY NMR experiment in  $[\text{D}_8]\text{THF}$  led again to responses in a single, albeit significantly smaller, range of diffusion coefficients of  $(1.4\text{--}3.8)\times 10^{-11} \text{ m}^2 \text{ s}^{-1}$ , in agreement with the larger hydrodynamic volume of the nano-objects in the better solvent (cf. the DLS results in Table 1). Therefore, within the sensitivity limits of the DOSY NMR experiment, we can conclude that the cross-linking reaction was complete.

The sensitivity of the phosphine groups to aerial oxidation to phosphine oxide was probed by exposure of **CCM** to air with monitoring by  $^{31}\text{P}\{^1\text{H}\}$  NMR spectroscopy. The spectrum of freshly synthesized **CCM** shows the phosphine resonance at  $\delta = -6.2$  ppm, while a second resonance at  $\delta = 24$  ppm corresponding to the phosphine oxide is barely visible ( $<1\%$  ac-

ording to the integration ratio of the two signals; see Supporting Information, Figure S2). The relative amount of the phosphine oxide increased to 14% after one week of exposure to air, and further to 32% after one month. When the same analyses were carried out under argon, no oxidation was detected.

The variation of the particle size of **CCM** was measured by DLS in water at  $20^\circ\text{C}$  as a function of pH (Figure 4). With increasing pH from 3.5 to 10.0,  $D_z$  slightly increases and then decreases, and the size range remains narrow (between 79 and

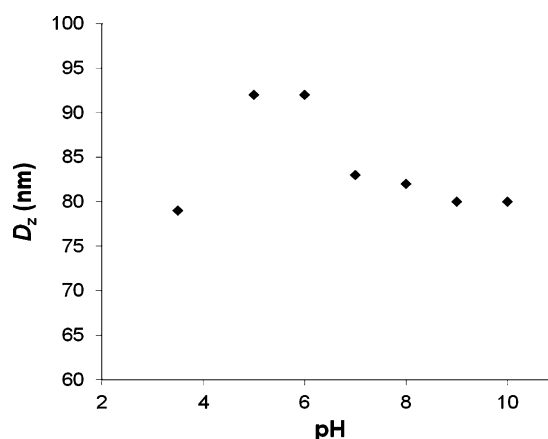


Figure 4. Evolution of the particle size with pH for **CCM** sample at  $20^\circ\text{C}$ .

92 nm). The slight increase in size with increasing pH can be attributed to deprotonation of the hydrophilic P(MAA-co-PEOMA) shell with formation of carboxylate anions and increasing solvation of these segments in water. Above pH 6, however, the increase in ionic strength presumably leads to screening of the charges and to the observed decrease in particle size. The particle size distribution is similar ( $0.15 \pm 0.03$ ) at all pH values. Neither precipitation nor aggregation was observed, and the latex remained stable whatever the pH.

As these particles are meant to be used in the biphasic olefin hydroformylation reaction, which is carried out at  $90^\circ\text{C}$  (see below), their stability as well as the stability of the dispersion was also evaluated as a function of temperature. The stability of **CCM** at  $90^\circ\text{C}$  was checked by stirring under argon for 5 d at pH 10 with particle-size monitoring by DLS measurements (Figure 5). The particle size increases with time and the polydispersity index (PDI) also increases, and this indicates a certain degree of particle aggregation under these harsh conditions. However, the overall dispersion remains stable and no coagulation was observed.

In conclusion, these preliminary tests confirmed that the **CCM** structure is stable at high pH and high temperature, with only a small extent of coagulation after prolonged heating (5 days at  $90^\circ\text{C}$ ).

### Mass transport of organic compounds into **CCM**

The unimolecular core-shell nano-objects reported herein have an unprecedented topology for catalytic applications.

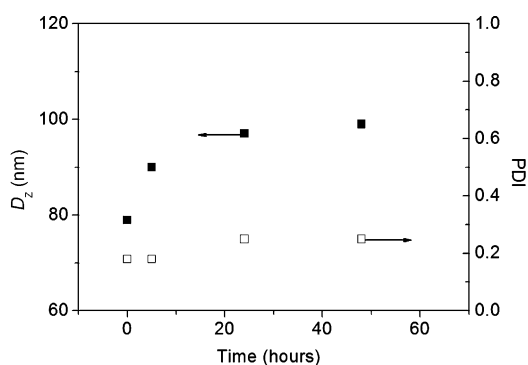


**Figure 5.** Stability testing of CCM at 90 °C and pH 10. Evolution of  $D_z$  and PDI with time.

Therefore, mass transport of hydrophobic molecules across the hydrophilic barrier required evaluation. A swelling test was performed for the CCM nanoreactors in the presence of 1-octene under the same conditions as used for the hydroformylation reaction (90 °C). CCM latex was mixed with the same volume of 1-octene and the mixture was heated at 90 °C without pH adjustment. Disappearance of the 1-octene phase after stirring suggested swelling of the CCM core by 1-octene, which was confirmed by the increase in particle size (i.e.,  $D_z=117$  nm after 20 h versus < 100 nm in the absence of 1-octene).

Swelling of the polymer core was also investigated by NMR spectroscopy in the presence of a variety of organic compounds at room temperature. Dilution of the CCM latex with  $D_2O$  and  $^1H$  NMR analysis led to the observation, in addition to a strong water resonance at  $\delta=4.70$  ppm, of a resonance at  $\delta=3.62$  ppm and a smaller one at  $\delta=3.30$  ppm, assigned respectively to the PEO methylene and terminal OMe protons of the hydrosoluble shell, whereas the signals of the aromatic protons in the polymer core are nearly invisible (spectrum a in Figure 6A). Note that the backbone  $CH_2$  and  $CH_3$  protons of the methacrylate units in the outer hydrophilic shell are also invisible, which suggests that these chains have greater affinity with the hydrophobic core and move in solidarity with it, with long correlation times. In addition, no resonance was observed in the  $^{31}P\{^1H\}$  NMR spectrum. Addition of  $CHCl_3$  to the latex, however, followed by brief stirring and immediate NMR monitoring, resulted in new spectra in which the core resonances could again be clearly observed, both by  $^1H$  and  $^{31}P\{^1H\}$  NMR spectroscopy (Figure 6B). The absence of a resonance at  $\delta=24$  ppm in the  $^{31}P\{^1H\}$  NMR spectrum confirms that no oxidation at the phosphorus atom took place during the polymerization and workup procedures. The strong and sharp resonance at  $\delta=7.15$  in the  $^1H$  spectrum is due to the  $CHCl_3$  molecules that have migrated inside the polymer particles. Integration of this resonance relative to that of the PEO methylene protons indicated that the nano-objects had incorporated about 2000 chloroform molecules per chain.

Core swelling was also evident on treatment with toluene (Figure 6C). In this case, in addition to the broad resonances of the PS aromatic protons, the  $^1H$  spectrum shows also sharp resonances for the encapsulated toluene molecules (multiplets for the aromatic protons around  $\delta=6.62$  and 6.72 ppm;

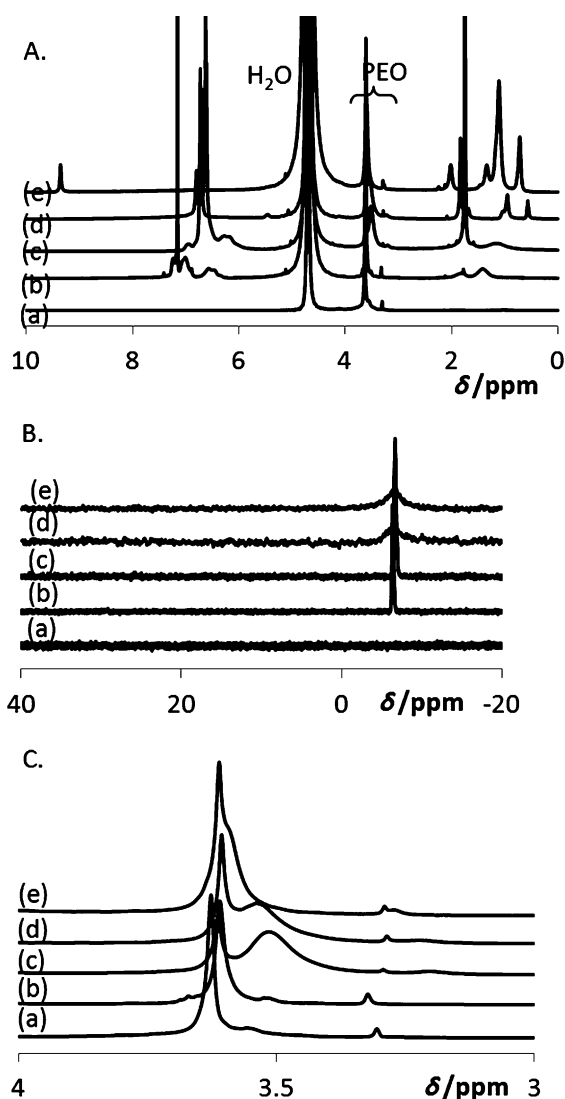


**Figure 6.**  $^1H$  (A) and  $^{31}P\{^1H\}$  (B) NMR spectra of CCM diluted in  $D_2O$ , before swelling (a) and after swelling with  $CHCl_3$  (b), toluene (c), 1/1 1-octene/toluene (d), and nonanal (e). C) Expansion of the PEO resonances in A.

methyl at  $\delta=1.74$  ppm). The resonances of the toluene-swollen core have slightly different chemical shifts to those of the  $CHCl_3$ -swollen core. The PEO methylene and terminal OMe resonances show an interesting phenomenon. Whereas they remain sharp for the  $CHCl_3$ -swollen sample (Figure 6B), each of them gives rise to a combination of a sharp resonance at the same chemical shift, but with reduced intensity, and a broader resonance centered at higher field ( $\delta=3.51$  ppm for the methylene protons and at  $\delta=3.20$  ppm for the OMe protons). These can be better seen in Figure 6C. The sum of the intensities corresponds to the expected total amount of PEO in the nano-object. This suggests that the greater part of the PEO chains are located inside the hydrophobic core when this is swollen by toluene. Deconvolution of the PEO methylene region as the sum of two Lorentzian functions (see Supporting Information, Figure S3) yielded a 30.3:69.7( $\pm 0.1$ ) ratio in favor of the core-confined resonance. Integration of the toluene aro-

matic and aliphatic protons against those of PEO indicated the presence of 770–950 toluene molecules per chain inside the nano-object. This number is only a rough estimate, since both toluene resonances, though sharp (see Figure 6), overlap with those of the core PS protons.

Treatment of **CCM** with pure 1-octene revealed neither the polymer-core resonances nor those of 1-octene itself. These peaks, however, became visible when the swelling was carried out with a 50/50 toluene/1-octene mixture (Figure 6d: CH(sp<sup>2</sup>) at  $\delta = 5.45$  ppm; CH(sp<sup>3</sup>) at  $\delta = 0.94$  ppm for methylene and 0.57 ppm for methyl). Therefore, whereas 1-octene is not able to diffuse into the polymer core when added as a pure phase at room temperature, it is able to do so when accompanied by a good solvent such as toluene. The overall solvent properties of the toluene/1-octene mixture are poorer than those of pure toluene for the **CCM** core, as indicated by the broader resonances of the core protons in the <sup>1</sup>H NMR spectrum and of the phosphine resonance in the <sup>31</sup>P{<sup>1</sup>H} NMR spectrum (Figure 6d). The core-confined PEO protons also give a broader resonance, centered around  $\delta = 3.58$  ppm in the <sup>1</sup>H NMR spectrum, the relative intensity of which is about the same as in toluene (72.4 ± 0.1 % of the total according to the deconvolution analysis, see Supporting Information, Figure S3). Integration of the solvent resonances (aromatic and aliphatic for toluene; vinylic and terminal methyl for octene) showed the presence of 420–520 molecules of toluene and 90–100 molecules of 1-octene per chain inside the polymer. These results are consistent with the known solubility properties of PS, which appear not to be significantly altered by the presence of 10% DPPS units: soluble in chloroform and toluene, insoluble in aliphatic hydrocarbons.

Finally, a swelling experiment was also carried out with nonanal, the expected product of 1-octene hydroformylation (Figure 6e), and decanal, used as solvent in the hydroformylation studies (the results with decanal are shown in Supporting Information, Figure S4). The behavior of these two organic additives is identical and similar to that of the toluene/octene mixture, as immediately suggested by the broadness of the phosphorus resonance. However, the total absence of visible core resonances in the <sup>1</sup>H NMR spectrum indicates that these long-chain aldehydes are even worse solvents for the hydrophobic core, although they are capable of swelling it, as shown by the typical resonances of the organic guest molecules, particularly that of the aldehydic proton at  $\delta = 9.35$  ppm. Integration suggested the presence of 150–180 molecules of nonanal (120–160 molecules of decanal) per chain inside the nano-object, depending on which signal intensity was used for the calculation. The PEO protons are once again split into sharper resonances for the chains in the aqueous environment and broader ones for those inside the polymer core (37.4:62.6 ± 0.1 % for nonanal and 33.1:66.9 ± 0.1 % for decanal, according to the deconvolution; see Supporting Information, Figure S3).

The most important information provided by these experiments, however, is the indication that mass transport of small organic molecules into the polymer core across the hydrophilic polymer shell barrier is a very rapid process, although the ki-

netics of this mass-transport phenomenon has not yet been investigated in greater detail.

### Coordination of [Rh(acac)(CO)<sub>2</sub>]

The next question of interest, addressed once again by NMR spectroscopy, is whether the nanoreactor can be charged with the desired precatalyst. Here, we focus only on hydroformylation, for which a commonly used precatalyst is [Rh(acac)(CO)<sub>2</sub>]. To transfer the precatalyst to the polymer core for the purpose of the NMR investigation, it was necessary to pre-swell the core with chloroform or toluene. Indeed, when the pristine (unswollen) latex was treated with a solution of [Rh(acac)(CO)<sub>2</sub>], we observed rapid crystallization of the complex as an orange solid, while the organic liquid phase disappeared due to migration into the polymer core. Treatment of the swollen latex with the same solution, on the other hand, resulted in complete transfer of the orange color from the organic phase to the aqueous phase on stirring for a few minutes at room temperature. <sup>31</sup>P{<sup>1</sup>H} NMR analysis confirmed that the Rh complex had coordinated to the phosphine groups in the polymer core to yield [Rh(acac)(CO)(PPh<sub>2</sub>-**CCM**)] (broad doublet at  $\delta = 47.5$  ppm,  $J_{\text{PRh}} = 175$  Hz, see Figure 7c) when a stoichio-

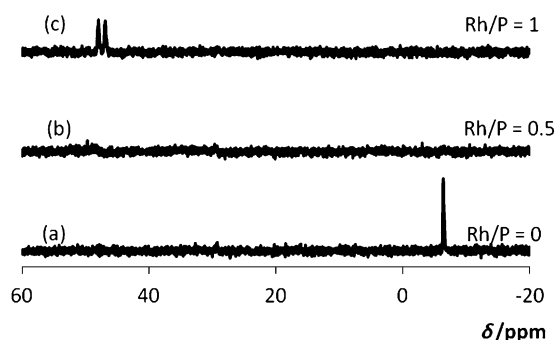


**Figure 7.** <sup>31</sup>P NMR spectra of the **CCM** latex after swelling with CHCl<sub>3</sub>, before (a) and after (b, c) treatment with a CHCl<sub>3</sub> solution of [Rh(acac)<sub>2</sub>(CO)<sub>2</sub>].

metric amount of Rh complex was used (Rh/P = 1) and complete disappearance of the resonance of the free phosphine. For comparison, the corresponding molecular complex [Rh(acac)(CO)(PPh<sub>3</sub>)] exhibits the <sup>31</sup>P{<sup>1</sup>H} resonance at  $\delta = 48.6$  ppm with  $J_{\text{PRh}} = 179.7$  Hz.<sup>[23]</sup> Interestingly, when half the amount of Rh complex was used (Rh/P = 0.5), neither the free-phosphine nor the coordinated-phosphine resonance was visible (Figure 7b). This is related to a resonance coalescence phenomenon because of rapid phosphine exchange, as previously demonstrated for the molecular complex.<sup>[24]</sup>

The thermal stability of the Rh-loaded latex was also checked. Disappointingly, immediate coagulation was observed on warming. We assume that this phenomenon is related to the thermal decarbonylation of the Rh center to yield [Rh(acac)(PPh<sub>2</sub>-polymer)<sub>2</sub>], analogous to the molecular complex with PPh<sub>3</sub>.<sup>[25]</sup> Hence, the Rh center may act as a cross-linking center between phosphine groups located not only on different arms within the same polymer particle, but also on differ-



ent polymer particles, which also indirectly suggests particle interpenetration. In spite of this negative result, we proceeded with testing of the nanoreactors in catalysis, in the hope that the CO-rich environment after precatalyst activation would disfavor cross-linking and maintain a well-dispersed polymer latex.

### Hydroformylation of 1-octene

To explore the catalytic potential of this new approach, **CCM** were used as nanoreactors for the rhodium-catalyzed hydroformylation of 1-octene as a model olefin substrate under biphasic conditions. This olefin has a sufficiently long chain to reduce its water solubility essentially to zero and to render the biphasic approach with molecular water-soluble Rh catalysts completely inefficient.<sup>[6]</sup> Hence, the hydroformylation of this substrate is a good model reaction to verify the efficiency of our new aqueous biphasic approach. It has also been extensively used to test other aqueous biphasic approaches, for example, with use of cosolvents,<sup>[26]</sup> calixarenes,<sup>[27]</sup> cyclodextrins,<sup>[7a]</sup> charged surfactants,<sup>[28]</sup> and polymer latexes<sup>[29]</sup> as additives, thermomorphic systems,<sup>[8c, e, 30]</sup> and micelles with the catalyst linked to the hydrophobic core.<sup>[31]</sup> As shown above, coordination of rhodium to the phosphine units leads to the appropriate hydroformylation precatalyst. The hydrophobic microenvironment inside the **CCM** is expected to be adequate for the reaction, without discarding possible beneficial confinement effects. Since a real alternative to existing technologies should remain as simple as possible, no cosolvents or surfactants were added to the reaction system. In order to directly compare the results with previous contributions on homogeneous hydroformylation with polymer ligands,<sup>[32]</sup> similar operating conditions were used (363 K and 20 bar of constant syngas pressure). Decanal was used as solvent to mimic the conditions of a continuous stirred-tank reactor, in which the composition of the outflowing organic-phase stream should mainly consist of C<sub>9</sub> aldehydes while preserving accurate quantification of the yield and selectivity of the recovered product phase by GC and NMR spectroscopy. The catalytically active species was generated *in situ* (see Experimental Section). The results are listed in Table 2.

In the first experiment (Table 2, run 1), the two-phase system recovered from the autoclave at the end of the reaction was composed of a lighter substrate/products solution and a heavier yellow aqueous phase. After overnight decantation, the clear organic solution showed no visible turbidity, that is, no significant **CCM** loss. The GC analysis indicated 94% 1-octene conversion (consistent with the syngas consumption when including sampling losses, see Figure 8) and an excellent mass balance ( $\approx 98\%$ ), and the major

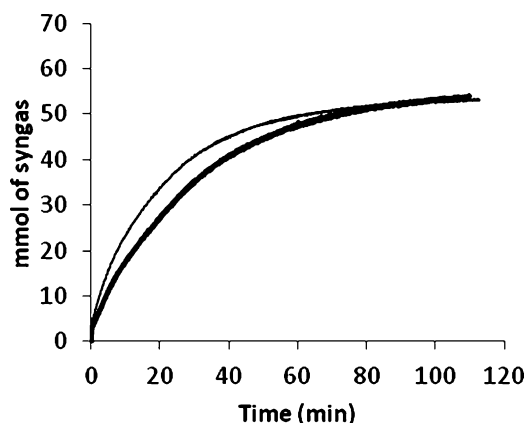


**Figure 8.** Monitoring of the syngas consumption for run 1 (bold line) and 1R (thin line) (Table 2).

products were the expected 1-nonanal and 2-methyl octanal in a linear-to-branched (l/b) ratio of about 5.0. Isomerization of 1-octene accounted for about 7% of the initial amount of substrate, whereas the hydrogenation byproducts (alkane and alcohols) were not observed. The imperfect mass balance may be rationalized by the permanence of a portion of the organic phase inside the swollen nanoparticles. Indeed, the recovered aqueous phase was more voluminous than that initially introduced into the autoclave. The initial turnover frequency (TOF) is higher than for other previously reported<sup>[33]</sup> experiments with immobilized Rh catalysts and rather close to those found with similar macroligands under homogeneous conditions,<sup>[32]</sup> although even higher activities have been reported in other cases (e.g., TOF up to 1200 h<sup>-1</sup> for a micellar approach at 70 °C with 30 bar syngas pressure<sup>[31]</sup> and up to 1550 h<sup>-1</sup> by Rh/TPPTS in the presence of surfactant additives at 100 °C and 20 bar syngas pressure<sup>[28b]</sup>). The rhodium loss, evaluated by ICP-MS analysis of the organic phase, was 1.8 ppm, corresponding to about 1% of the total amount.

The aqueous phase recovered from run 1, after resting while exposed to air under normal laboratory conditions for 5 d, was reintroduced into the autoclave for a second reaction (Table 2, run 1R), which was conducted under conditions identical to

**Table 2.** Results of the aqueous biphasic hydroformylation of 1-octene by [Rh(acac)(CO)<sub>2</sub>]/nano-object latex.<sup>[a]</sup>

Run	Nano-object	Additive	V <sub>Org</sub> /V <sub>Aq</sub>	t [min]	l/b <sup>[b]</sup>	TOF <sub>max</sub> [h <sup>-1</sup> ] <sup>[c]</sup>	Conv. [%] <sup>[d]</sup>	Yield [%] <sup>[d]</sup>	Leaching [ppm Rh]
1	<b>CCM</b>	–	2/1	110	5.0	628	94.7	93	1.8
1R	<b>CCM</b>	–	2/1	115	3.4	782	93.6	81.6	2.5
2	<b>CCM</b>	–	3/1	210	5.0	441	97.7	89.1	2.0
3	<b>CCM</b>	sulfoxantphos <sup>[e]</sup>	3/1	120	–	13	–	3.0 <sup>[f]</sup>	0.1
4	<b>M</b>	–	3/1	180	3.8	560	96.6	90.9	7.2

[a] Conditions: [1-octene]<sub>0</sub> = 1.1 mol L<sup>-1</sup> in the organic phase, 3.37 wt% of polymer content in the aqueous phase, T = 363 K, P<sub>syngas</sub> = 20 bar (CO/H<sub>2</sub> = 1), P/Rh = 4, 1-octene/Rh = 500, total liquid volume = 0.1 L. [b] From GC/FID analysis. [c] Turnover frequency, calculated from the initial syngas consumption (first 10 min). [d] 1-Octene conversion and total aldehyde yield (1-nonanal + 2-methyloctanal) measured by GC; the only observed byproducts were the octene isomers. [e] [Sulfoxantphos] = 0.033 mol L<sup>-1</sup> in the aqueous phase (sulfoxantphos/Rh = 5). [f] From the syngas consumption.

run 1. The results were also very similar (see Table 2 and Figure 8). Surprisingly, the initial reaction rate and TOF were even higher than those of run 1, but at the end of the run (120 min) the yields were very similar, whereas the I/b ratio was slightly lower. The Rh losses were also slightly greater (Table 2). Probably a fraction of the phosphine ligands was oxidized while resting, as suggested by the stability experiment (Supporting Information, Figure S2), and this led to less selective/faster catalytic intermediates. Nevertheless, the structure of the **CCM** seems to prevent extensive catalyst deactivation. This is in stark contrast to the molecular ligand. For instance, when propene was hydroformylated with sulfoxantphos as ligand, the catalyst decomposed unless always kept under hydroformylation conditions.<sup>[34]</sup>

In the light of the **CCM** swelling, we ran an additional experiment with a greater organic-to-aqueous phase ratio (run 2 in Table 2) to insure no phase inversion, i.e., to keep the catalytic phase dispersed into the substrate/products organic phase. Since the 1-octene/Rh molar ratio was kept constant at 500, this run had a higher catalyst concentration in the aqueous phase relative to run 1. Interestingly, the initial TOF in this run was reduced, probably because of mass transport limitations given the smaller amount of water dispersing the catalytic **CCM**. The gas consumption for this run is shown in Figure 9. Further investigations of this phenomenon will be reported elsewhere. The I/b ratio and rhodium leaching were not influenced by the phase volume ratio.

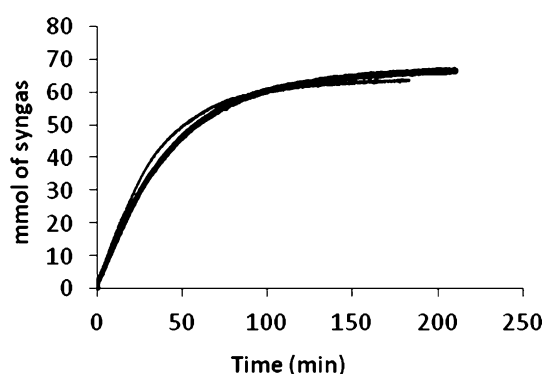


**Figure 9.** Comparison of the syngas consumption for catalysis with **CCM** (run 2, bold line) and **M** (run 4, thin line; Table 2).

So far, the catalytic tests have shown that mass transfer of the substrate to the catalytic sites is fast, that the **CCM** offers an adequate environment for fast hydroformylation reaction, and that the polymer scaffold protects the active sites against decomposition when stored in air. Given the insufficient solubility of 1-octene in water, the mass transport of the substrate to the catalytic site must be rendered possible by efficient stirring to favor extensive interfacial contact, rather than by molecular migration of the substrate through the aqueous phase. The hydrophilic P(MAA-co-PEOMA) shell of the **CCM** does not appear to represent a major obstacle against substrate and product transport into and out of the nanoreactor core (Figure 10A). However, efficient catalysis might also be alternative-

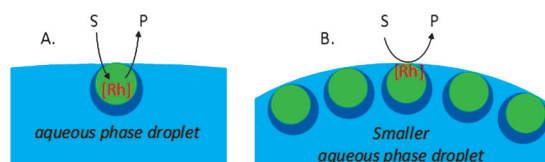


**Figure 10.** Alternative interpretations of the efficient catalytic biphasic hydroformylation in the presence of **CCM**: mass transport to the **CCM** core as in micellar catalysis (A) and increased surface area by surfactant effect for interfacial catalysis (B). S = substrate, P = product.

ly interpreted as a simple interfacial effect, whereby the **CCM** serves as a surfactant to stabilize the dispersion, and the catalytic transformation occurs at the greatly increased organic/water interface, but only through the Rh centers located at the **CCM** core/shell interface rather than through migration of the substrate to the **CCM** core (Figure 10B). To test this hypothesis, we carried out the hydroformylation in the presence of sulfoxantphos. This additive was chosen for several reasons: 1) it is water-soluble; 2) it has greater affinity for rhodium than the polymer-anchored phosphine; 3) it leads to a much greater I/b ratio in Rh-catalyzed hydroformylation. Thus, this ligand should be able to fully extract the rhodium catalyst from the **CCM** and, in the case of an efficient catalytic transformation, the measured I/b ratio should be a clear marker to indicate which ligand (the **CCM**-anchored PPh<sub>3</sub> or the sulfoxantphos in the aqueous phase) was involved in catalysis. At the same time, the Rh-free **CCM** should still be capable of providing the surfactant stabilization effect depicted in Figure 10B, which leads to an increased interfacial action by the water-soluble Rh/sulfoxantphos catalyst. We note that this phenomenon indeed accelerates the hydroformylation of higher alkenes (1-octene and 1-dodecene) by Rh/sulfoxantphos in the presence of polymer latexes and nonionic surfactants.<sup>[29]</sup>

The results of this experiment (Table 2, run 3) indicate that essentially no catalytic transformation occurs. Although an initial gas consumption was recorded, which could be related to slow equilibration of the gas-dissolution process, no significant amount of aldehyde product could be detected by GC. Note that the catalytic phase was prepared in the same way as for the previous experiments, that is, **CCM** was first swollen and charged with the [Rh(acac)(CO)<sub>2</sub>] precatalyst. Only after equilibration was the sulfoxantphos ligand introduced, at the same time as the substrate. Therefore, the catalytic results prove at the same time that the water-confined sulfoxantphos totally extracts the Rh complex from **CCM** and that any surfactant stabilization of the aqueous phase dispersion has no significant effect on catalysis. For comparison, the biphasic hydroformylation of 1-octene by [Rh(acac)(CO)<sub>2</sub>]/sulfoxantphos in the absence of any additives was reported to yield 19% conversion with catalyst and substrate amounts similar to ours (1-octene/Rh = 500, sulfoxantphos/Rh = 5), but only after 24 h and under much harsher conditions (120 °C and 50 bar syngas pressure) than those used in our experiment.<sup>[7a]</sup> The reason for the absence of interfacial acceleration by our **CCM**, in contrast to the reported strong effect of other polymer latexes,<sup>[29]</sup> for hydroformylation by aqueous Rh-sulfoxantphos may be attributed to

the thicker hydrophilic layer separating the **CCM** core, where 1-octene is located, and the aqueous phase carrying the catalyst. We therefore conclude that **CCM** probably operates as a unimolecular micelle and that the catalysis takes place in the non-cross-linked part of the particle core, with substrate and product transport into and out of the nanoreactor, as represented in Figure 10A. Note that coordination of Rh to sulfoxantphos also led to much less leaching into the organic phase, which might be due to a lower solubility of this ligand in the organic phase and/or a stronger coordination of the metal.

Finally, a catalytic test was also carried out under the same conditions with the **M** latex (Table 2, run 4 and Figure 9), and showed a minimal reaction-rate gain relative to the performance of the **CCM** under the same conditions ( $V_{\text{Org}}/V_{\text{Aq}}=3/1$ , cf. Table 2, runs 2 and 4), accompanied by a much more substantial loss of rhodium into the organic phase. This result was expected because of the instability of the non-cross-linked nanoreactors, and validates our choice of the globular cross-linked architecture of the **CCM**.

## Conclusion

We have introduced a new catalytic tool for application to biphasic catalytic transformations, based on the principle of micellar catalysis but replacing the micelle with a core-cross-linked unimolecular nanoreactor. The nano-objects are assembled by a convenient and scalable one-pot process in three steps and obtained as latex directly usable in catalysis. Physicochemical investigations demonstrated particle uniformity, latex stability, facile mass transport of organic molecules across the hydrophilic barrier, and rapid incorporation and coordination of a transition metal precatalyst. The objects were applied to a challenging transformation of industrial interest, namely, the biphasic hydroformylation of higher olefins, for which 1-octene was used as a model substrate, and efficiency, ease of product separation, and recyclability were demonstrated. Furthermore, the nanoreactors were shown to provide a protecting environment for the fragile catalyst in air. Catalyst leaching (ca. 2 ppm) was substantially reduced relative to the equivalent non-cross-linked micelle but requires further improvement. The causes for this leaching are currently under investigation, as well as further optimization of the polymer architecture.

## Experimental Section

### Materials

4,4'-Azobis(4-cyanopentanoic acid) (ACPA, >98%, Fluka), methacrylic acid (MAA, 99.5%, Acros), poly(ethylene oxide) methyl ether methacrylate (PEOMA,  $M_n=950 \text{ g mol}^{-1}$ , Aldrich), diethylene glycol dimethacrylate (DEGDMA, 95%, Aldrich), 4-diphenylphosphinostyrene (DPPS, 97%, Aldrich), 1,3,5-trioxane (Aldrich, >99%) [Rh(acac)(CO)<sub>2</sub>] (99%, Alfa Aesar), 1-octene (99+%, Acros), *n*-nonanal (>97%, Alfa Aesar), *n*-decanal (>96%, Alfa Aesar), and anisole (99%, Fluka) were used as received. Styrene (S, 99%, Acros) was purified by passing it through a column of active basic aluminum oxide to remove the stabilizer. The RAFT agent 4-cyano-4-thiothiopropylsulfanyl pentanoic acid (CTPPA) was synthesized as de-

scribed previously.<sup>[35]</sup> Deionized water (Purelab Classic UV, Elga Lab-Water) was used in this work. Carbon monoxide and dihydrogen were obtained from Linde Gas. Syngas was prepared by introducing equimolar amounts of CO and H<sub>2</sub> into a monitored gas reservoir feeding the autoclave reactor at constant pressure. A Hastelloy C276 autoclave equipped with a gas-inducing stirrer was used for the hydroformylation experiments. All chemical structures are shown in the Supporting Information (Scheme S1).

### Preparation of micelles (M) and core-cross-linked micelles (CCM) through one-pot RAFT polymerization in aqueous media

The typical procedure for the synthesis of **CCM** is as follows (see Table 1, Run 2).

**Step 1: Preparation of P(MAA-co-PEOMA)-TTC macromolecular RAFT agent (macroRAFT) in water:** A stock solution containing ACPA (10 mg g<sup>-1</sup>) and NaHCO<sub>3</sub> (1.5 M) in deionized water was prepared. 0.8 g of this stock solution (8 mg ACPA, 0.0285 mmol), 40 mg of CTPPA (0.145 mmol), 189 mg of MAA (2.19 mmol), 2.091 g of PEOMA (2.23 mmol), and 8.79 g of deionized water (including the water of the ACPA solution) were added to a 50 mL flask with a magnetic bar. 1,3,5-Trioxane (19.7 mg, 0.219 mmol) was also added to the flask as an internal reference for determination of the monomer conversion by <sup>1</sup>H NMR. The solution in the septum-sealed flask was purged for 45 min with argon and then heated to 80 °C in a thermostated oil bath under stirring. After 120 min, 0.15 mL of solution was taken to determine the monomer conversion and the molar mass of the macroRAFT. The overall monomer molar conversion was about 99%, as determined by <sup>1</sup>H NMR spectroscopy in [D<sub>6</sub>]DMSO. The molar mass was analyzed by size exclusion chromatography (SEC) in DMF (experimental  $M_n=16\,200 \text{ g mol}^{-1}$ ;  $\mathcal{D}=1.11$ ).

**Step 2: RAFT copolymerization of S and DPPS in water:** During the polymerization of Step 1, S (4.253 g, 40.8 mmol) and DPPS (0.622 g, 2.16 mmol) were dispersed in 10.66 g of deionized water, to which was also added the ACPA stock solution (0.8 g containing 8 mg of ACPA, 0.0285 mmol). Then the mixture was purged for 45 min with argon at 0 °C. After the sampling of step 1, the mixture was quickly injected into the flask under argon at 80 °C. After 3 h, 0.5 mL of solution was withdrawn for analysis and the polymerization was quenched by immersion of the flask in iced water. The overall conversion of S (97%) was determined by gravimetric analysis, and that of DPPS (100%) by <sup>31</sup>P NMR spectroscopy in [D<sub>8</sub>]THF.

**Step 3: Cross-linking in the particle core:** To the flask containing the P(MAA-co-PEOMA)-*b*-P(S-co-DPPS) latex from step 2, S (1.285 g, 12.34 mmol), DEGDMA (0.337 g, 1.39 mmol), 0.77 g of the ACPA stock solution (7.7 mg of ACPA, 0.027 mmol), and 6.82 g of deionized water were added. The mixture was purged for 1 h with argon at 0 °C, and the flask was then placed in an oil bath thermostated at 80 °C. After 1 h, the polymerization was quenched by immersion of the flask in iced water. The overall conversion of the comonomers (100%) was determined by gravimetric analysis.

The same procedure was employed in the preparation of **CCM** without DPPS; the amount of styrene was adjusted to 2 mol per liter of water (4.452 g, 42.8 mmol) in step 2 (Supporting Information, Table S1). The synthesis of micelles **M** was performed by following steps 1 and 2 in the presence of the total amount of styrene in step 2 (run 1, Table 1).

## Hydroformylation of 1-octene under biphasic conditions

**With CCM latex, organic/aqueous phase = 2/1 (v/v):** Deionized water (32 mL) was introduced into a Schlenk tube and degassed by bubbling with dinitrogen. The desired quantity of CCM latex (4.5 mL, 0.58 mmol of phosphorus) was added through a nitrogen-purged syringe and the resulting mixture was stirred for 15 min. To swell the hydrophobic nanoparticle core, 3 mL of decanal was added and the colloidal suspension was stirred for a further 15 min. Then, a separate solution containing  $[\text{Rh}(\text{acac})(\text{CO})_2]$  (38 mg, 0.144 mmol) in 3 mL of decanal was added through a Teflon cannula and the resulting mixture was stirred for 5 min. This mixture (the "aqueous phase") was then transferred into the autoclave, followed by the addition of the remaining decanal (49 mL) and 1-octene (8.09 g, 11.3 mL, 72 mmol). The system was purged three times with 15 bar of nitrogen, then four times with 15 bar of syngas. The reactor was subsequently heated under low syngas pressure (2 bar) and slow stirring speed (300 rpm, well below gas self-induction) to hinder significant gas dissolution and the start of the reaction. When the desired reaction temperature (90 °C) was achieved, stirring was stopped and the autoclave was pressurized at the desired syngas pressure (20 bar). A sample was withdrawn to evaluate the amount of products formed during the heating procedure by GC/FID analysis. Then, the data acquisition was started and the stirring speed was set to 1200 rpm. During the course of the reaction, the autoclave was constantly fed with syngas at 20 bar from a ballast. Both temperature and pressure of the reactor and the gas ballast were recorded on-line on a computer at a rate of 1 Hz. The instantaneous reaction rate was measured from the syngas consumption calculated from the ballast pressure drop. After 2 h heating was stopped and the autoclave cooled at low stirring speed (200 rpm). Once the autoclave was cold, the reactor was purged with nitrogen four times. The mixture in the reactor was taken out and transferred to a separating funnel for decantation overnight in air. For GC analyses, a precise quantity of anisole (internal standard) was added before dilution with diethyl ether and injection into the gas chromatograph. The identity of the reaction components (1-octene, *n*-nonanal, 2-methyloctanal, and *n*-decanal) was confirmed by GC-MS analysis.

**Recycling test:** After 5 d in air, the residual aqueous catalytic phase (46 mL) from the above run was reintroduced into the reactor. Then, fresh 1-octene (8.09 g, 72 mmol) and *n*-decanal (41 mL) were poured directly into the reactor. The reactor was then purged with 15 bar of nitrogen three times followed by 15 bar of syngas four times. The experiment was then continued as described above.

**With CCM latex, organic/aqueous phase = 3/1 (v/v):** The procedure was identical to that described above, except for the relative amounts of the reagents: water (20 mL), CCM latex (5 mL, 0.65 mmol of P),  $[\text{Rh}(\text{acac})(\text{CO})_2]$  (43 mg, 0.16 mmol), 1-octene (9.17 g, 12.8 mL, 82 mmol), and decanal (62 mL, 51.4 g). The reaction was stopped after 3 h.

**With M latex:** For micellar catalysis, the same procedure as mentioned above was followed, by using 5 mL of M latex (0.65 mmol of P).

**With CCM latex in the presence of sulfoxantphos:** The aqueous phase containing CCM latex (0.65 mmol of P) and rhodium precursor (0.16 mmol) was prepared as described above by using 15 mL of water. It was introduced into the autoclave and heated to 70 °C under syngas ( $\approx$ 2 bar) to yield the catalytic complex, then allowed to cool. Sulfoxantphos (645 mg, 1.65 mmol of P) was dissolved in 5 mL of water. It was added simultaneously with the organic phase to the autoclave from a dropping funnel under nitrogen pressure.

The biphasic mixture was heated under low syngas pressure (2 bar) and at slow stirring speed (300 rpm) to 90 °C. The hydroformylation reaction was then performed as usual (90 °C, 20 bar syngas, stirring speed of 1200 rpm) for 2 h.

## Characterization techniques

**NMR spectroscopy:**  $^1\text{H}$  NMR and  $^{31}\text{P}$  NMR measurements were performed in 5 mm-diameter tubes in  $[\text{D}_6]$ DMSO or  $[\text{D}_6]$ THF solution (the aliquots of the polymerization medium were directly dissolved in the solvent) at 25 °C on a Bruker Avance 300 spectrometer. For CCM characterization, 1 mL of latex was dried under vacuum until a white paste was obtained, which was dispersed in  $[\text{D}_6]$ DMSO or in  $[\text{D}_6]$ THF in an NMR tube (5 mm). The chemical shift scale was calibrated on the basis of the solvent peak ( $\delta = 2.50$  ppm for DMSO;  $\delta = 3.58$  and 1.73 ppm for THF), and 1,3,5-trioxane was used as an integration reference ( $\delta = 5.20$  ppm). The quantitative  $^{31}\text{P}$  NMR assay used the zgpg pulse program, with adequate impulsion time and attenuation, and adjusted relaxation delay. The accuracy of the determination was verified with standard solutions of  $\text{Ph}_3\text{PO}$  (estimated error:  $\pm 2\%$ ). The  $^1\text{H}$  DOSY NMR study on CCM in water was carried out in a 5 mm-diameter tube equipped with a  $\text{D}_2\text{O}$  capillary at 20 °C, by using the stebpgp1s19s pulse program with usual parameters (Big Delta  $\text{D}20 = 140$  ms and  $\text{P}30 = 1400$   $\mu\text{s}$  or  $5.08$   $\text{Gmm}^{-1}$ ). In the case of the  $^1\text{H}$  DOSY NMR experiments on CCM in  $[\text{D}_6]$ THF, 0.1 mL of latex was evaporated to dryness at room temperature under reduced pressure until a white paste was obtained, which was dispersed in  $[\text{D}_6]$ THF. A similar approach for data acquisition was used with the stebpgp1s pulse program with  $\text{D}20 = 100$  ms and  $\text{P}30 = 1000$   $\mu\text{s}$ .

**Size exclusion chromatography:** SEC was performed in DMF ( $+0.01$   $\text{molL}^{-1}$  LiBr, with toluene as a flow-rate marker) at 50 °C and a flow rate of  $1.0$   $\text{mLmin}^{-1}$  by using a Viscotek TDA305 apparatus (SEC-DMF). All polymers were analyzed at a concentration of  $3$   $\text{mgmL}^{-1}$  after filtration through a membrane with  $0.45$   $\mu\text{m}$  pore size. The separation was carried out on three columns from PSS GRAM ( $7$   $\mu\text{m}$ ,  $300 \times 7.5$  mm). The setup was equipped with a refractive-index (RI) detector ( $\lambda = 670$  nm). The average molar masses (number-average molar mass  $M_n$  and weight-average molar mass  $M_w$ ) and the dispersity ( $\mathcal{D} = M_w/M_n$ ) were derived from the RI signal by a calibration curve based on poly(methyl methacrylate) standards (PMMA from Polymer Laboratories) for the analysis of the methylated P(MAA-co-PEOMA)-TTC macroRAFT<sup>[18c]</sup> and on polystyrene standards (PS from Polymer Laboratories) for the analysis of the block copolymers. The software used for data collection and calculation was OmniSec version 4.7 from Malvern Instruments.

**DLS:** The intensity-average diameters of the latex particles  $D_z$  and PDI were measured by DLS with a Zetasizer Nano Series (Nano ZS) from Malvern Instrument by using the Zetasizer 6.2 software. The instrument was calibrated with a standard polystyrene latex in water exhibiting a particle size of  $220 \pm 6$  nm. Before measurements, the latex samples were diluted with deionized water. Different series of analyses on the final samples were carried out at 20 °C while varying the pH from 3.5 to 10 by adjustment with 1 N solutions of NaOH or HCl. A few measurements were also carried out with samples swollen with 1-octene.

**TEM:** The morphologies of the dispersions of diblock copolymer nano-objects were studied by TEM. Diluted latex samples were dropped on a Formvar/carbon-coated copper grid and dried under air. The samples were examined with a Philips CM120 transmission electron microscope operating at 80 kV (Centre Technologique des Microstructures (CT $\mu$ ), platform of the Université Claude Bernard Lyon 1, Villeurbanne, France).

**GC:** GC was carried out on a Thermo Fisher Trace GC 2000 chromatograph equipped with a CB-CP WAX 52 capillary column (25 m × 0.25 mm, 0.2 μm film thickness) and a flame ionization detector (FID) with helium as carrier gas.

**High-resolution ICP-MS:** Leaching of the rhodium catalyst in the organic phase was measured by high-resolution ICP-MS on a XR Thermo Scientific Element. For sample preparation, the recovered organic phase was diluted in water with a volumetric dilution factor of 10<sup>5</sup>. In practice, a 1 L volumetric flask was filled to about two-thirds with milli-Q water, and then 10 μL of the organic product phase was introduced by using a Gilson P20 precision pipette. The borders were rinsed and the flask was introduced into an ultrasound bath for 30 min. The solution was left overnight and the dilution was then completed with milli-Q water to the 1 L mark. Standards were prepared using solutions of [Rh(acac)(CO)<sub>2</sub>] in *n*-decanal with various weight fractions of Rh in the (0.001–0.5) × 10<sup>-9</sup> range (1–500 ppt).

## Acknowledgements

We are grateful to the Agence Nationale de la Recherche (ANR) for support of this work through grant “BIPHASNANO-CAT” (ANR-11-BS07-025-01). Additional support from the Centre National de la Recherche Scientifique (CNRS) and from the Institut Universitaire de France (IUF) is also gratefully acknowledged. We thank Prof. P. W. N. M. Van Leeuwen for a generous gift of sulfoxantphos.

**Keywords:** biphasic catalysis · hydroformylation · polymerization · rhodium · self-assembly

- [1] a) J. A. Moulijn, M. T. Kreutzer, T. A. Nijhuis, F. Kapteijn in *Monolithic Catalysts and Reactors: High Precision with Low Energy Consumption*, Vol. 54 Eds.: B. C. Gates, H. Knozinger, **2011**, pp. 249–327; b) Y. Sumino, T. Fukuyama, *J. Synth. Org. Chem. Jpn.* **2012**, *70*, 896–907; c) A. Puglisi, M. Benaglia, V. Chiroli, *Green Chem.* **2013**, *15*, 1790–1813; d) D. B. Zhao, K. L. Ding, *ACS Catal.* **2013**, *3*, 928–944.
- [2] a) I. T. Horvath, J. Rabai, *Science* **1994**, *266*, 72–75; b) D. F. Foster, D. Gudmunsen, D. J. Adams, A. M. Stuart, E. G. Hope, D. J. Cole-Hamilton, G. P. Schwarz, P. Pogorzelec, *Tetrahedron* **2002**, *58*, 3901–3910.
- [3] a) T. Welton, *Chem. Rev.* **1999**, *99*, 2071–2084; b) P. Wasserscheid, W. Keim, *Angew. Chem. Int. Ed. Engl.* **2000**, *39*, 3772–3789; c) C. Kolbeck, N. Paape, T. Cremer, P. S. Schulz, F. Maier, H. P. Steinruck, P. Wasserscheid, *Chem. Eur. J.* **2010**, *16*, 12083–12087; d) A. Sharma, C. Julcour-Lebigue, R. M. Deshpande, A. A. Kelkar, H. Delmas, *Ind. Eng. Chem. Res.* **2010**, *49*, 10698–10706.
- [4] B. Cornils, *Org. Process Res. Dev.* **1998**, *2*, 121–127.
- [5] C. W. Kohlpaintner, R. W. Fischer, B. Cornils, *Appl. Catal. A* **2001**, *221*, 219–225.
- [6] R. M. Deshpande, P. Purwanto, H. Delmas, R. V. Chaudhari, *Ind. Eng. Chem. Res.* **1996**, *35*, 3927–3933.
- [7] a) L. Leclercq, F. Hapiot, S. Tilloy, K. Ramkisoensing, J. N. H. Reek, P. W. N. M. van Leeuwen, E. Monflier, *Organometallics* **2005**, *24*, 2070–2075; b) F. X. Legrand, F. Hapiot, S. Tilloy, A. Guerriero, M. Peruzzini, L. Gonsalvi, E. Monflier, *Appl. Catal. A* **2009**, *362*, 62–66.
- [8] a) A. Behr, *Multiph. Homog. Catal.* **2005**, *1*, 327–329; b) H. Hamamoto, Y. Suzuki, Y. M. A. Yamada, H. Tabata, H. Takahashi, S. Ikegami, *Angew. Chem.* **2005**, *117*, 4612–4614; *Angew. Chem. Int. Ed.* **2005**, *44*, 4536–4538; c) J. Tijani, B. ElAli, *Appl. Catal. A* **2006**, *303*, 158–165; d) A. Behr, G. Henze, R. Schomaecker, *Adv. Synth. Catal.* **2006**, *348*, 1485–1495; e) E. Hermanns, J. Hasenjaeger, B. Driessen-Hoelscher, *Top. Organomet. Chem.* **2008**, *23*, 53–66.
- [9] a) G. Oehme, *Appl. Homogeneous Catal. Organomet. Compd.* **2002**, *2*, 835–841; b) V. C. Reinsborough, *Interf. Catal.* **2003**, 377–390; c) M. N. Khan, *Micellar Catalysis*, CRC Press, **2006**, p. 464 pp.
- [10] P. Cotanda, N. Petzetakis, R. K. O'Reilly, *MRS Commun.* **2012**, *2*, 119–126.
- [11] a) R. K. O'Reilly, C. J. Hawker, K. L. Wooley, *Chem. Soc. Rev.* **2006**, *35*, 1068–1083; b) H. Gao, K. Matyjaszewski, *Progr. Polym. Sci.* **2009**, *34*, 317–350.
- [12] A. D. Levins, X. F. Wang, A. O. Moughton, J. Skey, R. K. O'Reilly, *Macromolecules* **2008**, *41*, 2998–3006.
- [13] Y. Liu, Y. Wang, Y. F. Wang, J. Lu, V. Pinon, M. Weck, *J. Am. Chem. Soc.* **2011**, *133*, 14260–14263.
- [14] a) T. Terashima, M. Kamigaito, K.-Y. Baek, T. Ando, M. Sawamoto, *J. Am. Chem. Soc.* **2003**, *125*, 5288–5289; b) T. Terashima, M. Ouchi, T. Ando, M. Kamigaito, M. Sawamoto, *J. Polym. Sci. Part A J. Polym. Sci. Polym. Chem.* **2006**, *44*, 4966–4980; c) T. Terashima, M. Ouchi, T. Ando, M. Kamigaito, M. Sawamoto, *Macromolecules* **2007**, *40*, 3581–3588.
- [15] T. Terashima, A. Nomura, M. Ito, M. Ouchi, M. Sawamoto, *Angew. Chem.* **2011**, *123*, 8038–8041; *Angew. Chem. Int. Ed.* **2011**, *50*, 7892–7895.
- [16] a) T. Terashima, M. Ouchi, T. Ando, M. Sawamoto, *J. Polym. Sci. Part A* **2010**, *48*, 373–379; b) T. Terashima, M. Ouchi, T. Ando, M. Sawamoto, *Polym. J.* **2011**, *43*, 770–777; c) T. Terashima, M. Ouchi, T. Ando, M. Sawamoto, *J. Polym. Sci. Part A* **2011**, *49*, 1061–1069.
- [17] a) B. Charleux, G. Delaittre, J. Rieger, F. D'Agosto, *Macromolecules* **2012**, *45*, 6753–6765; b) J.-T. Sun, C.-Y. Hong, C.-Y. Pan, *Polym. Chem.* **2013**, *4*, 873–881.
- [18] a) I. Chaduc, W. Zhang, J. Rieger, M. Lansalot, F. D'Agosto, B. Charleux, *Macromol. Rapid Commun.* **2011**, *32*, 1270–1276; b) X. Zhang, S. Boissé, W. Zhang, P. Beaunier, F. D'Agosto, J. Rieger, B. Charleux, *Macromolecules* **2011**, *44*, 4149–4158; c) W. Zhang, F. D'Agosto, O. Boyron, J. Rieger, B. Charleux, *Macromolecules* **2011**, *44*, 7584–7593; d) I. Chaduc, M. Girod, R. Antoine, B. Charleux, F. D'Agosto, M. Lansalot, *Macromolecules* **2012**, *45*, 5881–5893; e) X. Zhang, J. Rieger, B. Charleux, *Polym. Chem.* **2012**, *3*, 1502–1509; f) W. Zhang, F. D'Agosto, O. Boyron, J. Rieger, B. Charleux, *Macromolecules* **2012**, *45*, 4075–4084; g) I. Chaduc, A. Crepet, O. Boyron, B. Charleux, F. D'Agosto, M. Lansalot, *Macromolecules* **2013**, *46*, 6013–6023; h) W. Zhang, F. D'Agosto, P.-Y. Dugas, J. Rieger, B. Charleux, *Polymer* **2013**, *54*, 2011–2019; i) M. Chenal, L. Bouteiller, J. Rieger, *Polym. Chem.* **2013**, *4*, 752–762; j) J. Xu, X. Xiao, Y. Zhang, W. Zhang, P. Sun, *J. Polym. Sci. Part A* **2013**, *51*, 1147–1161; k) E. Velasquez, J. Rieger, F. Stoffelbach, B. Charleux, F. D'Agosto, M. Lansalot, P.-E. Dufils, J. Vinas, *Polymer* **2013**, *54*, 6547–6554.
- [19] Y. Mai, A. Eisenberg, *Chem. Soc. Rev.* **2012**, *41*, 5969–5985.
- [20] a) A. Blencowe, J. F. Tan, T. K. Goh, G. G. Qiao, *Polymer* **2009**, *50*, 5–32; b) N. Sanson, J. Rieger, *Polym. Chem.* **2010**, *1*, 965–977; c) Z. An, Q. Qiu, G. Liu, *Chem. Commun.* **2011**, *47*, 12424–12440; d) Q. J. Chen, X. T. Cao, Y. Y. Xu, Z. S. An, *Macromol. Rapid Commun.* **2013**, *34*, 1507–1517.
- [21] a) J. Rieger, C. Grazon, B. Charleux, D. Alaimo, C. Jérôme, *J. Polym. Sci. Part A* **2009**, *47*, 2373–2390; b) C. Grazon, J. Rieger, N. Sanson, B. Charleux, *Soft Matter* **2011**, *7*, 3482–3490; c) G. Liu, Q. Qiu, W. Shen, Z. An, *Macromolecules* **2011**, *44*, 5237–5245; d) Q. Qiu, G. Liu, Z. An, *Chem. Commun.* **2011**, *47*, 12685–12687; e) W. Shen, Y. Chang, G. Liu, H. Wang, A. Cao, Z. An, *Macromolecules* **2011**, *44*, 2524–2530; f) Q. Chen, X. Cao, H. Liu, W. Zhou, L. Qin, Z. An, *Polym. Chem.* **2013**, *4*, 4092–4102.
- [22] C. S. Johnson, *Progr. Nucl. Magn. Res. Spectr.* **1999**, *34*, 203–256.
- [23] F. Bonati, G. Wilkinson, *J. Chem. Soc.* **1964**, 3156–3160.
- [24] A. M. Trzeciak, M. Jon, J. J. Ziolkowski, *React. Kinet. Catal. Lett.* **1982**, *20*, 383–387.
- [25] A. J. Mukhedkar, V. A. Mukhedka, M. Green, F. G. A. Stone, *J. Chem. Soc. A* **1970**, 3166–3171.
- [26] a) I. Hablot, J. Jenck, G. Casamatta, H. Delmas, *Chem. Eng. Sci.* **1992**, *47*, 2689–2694; b) P. Kalck, P. Escaffre, F. Sereinspirau, A. Thorez, B. Besson, Y. Colleuille, R. Perron, *New J. Chem.* **1988**, *12*, 687–690.
- [27] S. Shimizu, S. Shirakawa, Y. Sasaki, C. Hirai, *Angew. Chem.* **2000**, *112*, 1313–1315; *Angew. Chem. Int. Ed.* **2000**, *39*, 1256.
- [28] a) S. L. Desset, D. J. Cole-Hamilton, D. F. Foster, *Chem. Commun.* **2007**, 1933–1935; b) S. L. Desset, S. W. Reader, D. J. Cole-Hamilton, *Green Chem.* **2009**, *11*, 630–637.
- [29] H. Nowothnick, A. Rost, T. Hamerla, R. Schomacker, C. Muller, D. Vogt, *Catal. Sci. Technol.* **2013**, *3*, 600–605.
- [30] M. S. Shaharun, B. K. Dutta, H. Mukhtar, S. Maitra, *Chem. Eng. Sci.* **2010**, *65*, 273–281.

- [31] G. M. Pawar, J. Weckesser, S. Blechert, M. R. Buchmeiser, *Beilstein J. Org. Chem.* **2010**, *6*, 28.
- [32] a) A. F. Cardozo, E. Manoury, C. Julcour, J.-F. Blanco, H. Delmas, F. Gayet, R. Poli, *ChemCatChem* **2013**, *5*, 1161–1169; b) A. F. Cardozo, E. Manoury, C. Julcour, J.-F. Blanco, H. Delmas, F. Gayet, R. Poli, *Dalton Trans.* **2013**, *42*, 9148–9156.
- [33] D. J. Cole-Hamilton, *Science* **2003**, *299*, 1702–1706.
- [34] M. S. Goedheijt, P. C. J. Kamer, P. van Leeuwen, *J. Mol. Catal. A* **1998**, *134*, 243–249.
- [35] a) X. Xu, A. E. Smith, S. E. Kirkland, C. L. McCormick, *Macromolecules* **2008**, *41*, 8429–8435; b) T. Boursier, I. Chaduc, J. Rieger, F. D'Agosto, M. Lansalot, B. Charleux, *Polym. Chem.* **2011**, *2*, 355–362.
- 
-